BEHAVIOUR OF THE BOTTOM AND TOP FLANGE PLATES IN THE SLIDING HINGE JOINT

Hsen-Han Khoo[1], Chris Seal[2], Charles Clifton[3], John Butterworth[3] and Gregory A. MacRae[4]

SUMMARY

The Sliding Hinge Joint is a low damage beam-column connection used in steel moment resisting frames. It dissipates energy through sliding in Asymmetric Friction Connections (AFCs) in the bottom web and bottom flange bolt groups. The AFC confines earthquake induced damage to bolts that can be retightened or replaced following a major earthquake. The other joint components sustain negligible damage and would be kept in service and may thus be subjected to further earthquake shaking during the lifetime of the building. The bottom and top flange plates are also subject to inelastic action about their minor axis under joint rotation. This study evaluates the behaviour of the bottom and top flange plates to determine the weld and plate susceptibility to low-cycle fatigue failure. The basic flange plate deformation was approximated by an arc, with the effects of shear slip considered to obtain estimates of likely strain demands. It was shown that even in the most critical case the fatigue life is more than six times the demand expected in a design level earthquake. As a result, it is concluded that properly designed, detailed and connected flange plates are not prone to low-cycle fatigue failure.

1. INTRODUCTION

The Sliding Hinge Joint (SHJ) is a beam-column connection used in steel moment resisting frames (MRFs). It was developed by Clifton [1] as a low-damage alternative to traditional welded connections. The joint layout is shown in Figure 1. The beam is pinned to the column through the top flange plate, which acts as the point of rotation, with Asymmetric Friction Connections (AFCs) in the bottom web and bottom flange bolt groups. The SHJ can undergo large inelastic rotations with minimal damage while decoupling MRF strength and stiffness. This is achieved through AFC sliding during SHJ rotation which minimises inelastic demand in the beam and columns. Most other joint components such as the web and flange plates sustain minimal damage. The AFCs are designed to be rigid under serviceability level earthquake (SLE) events and slide under design level earthquake (DLE) events. When this occurs, the bolts are subject to additional plasticity which results in a drop in tension. Under maximum considered earthquake (MCE) events, the bolts may hit the end of the slotted holes, which would increase the joint resistance but also result in further bolt tension loss. The SHJ retains flexural resistance provided the bolts are sized to ensure further deformation occurs through ductile yielding of the plates. The pinning of the beam to the column about the top flange plate minimises beam elongation and damage to the floor slab. The benefits of the SHJ over welded connections include (1) decoupled moment frame strength and stiffness, (2) confinement of inelastic demand to the bolts which are easily replaced following an earthquake, (3) improved seismic-dynamic recentering ability, and (4) lower cost.

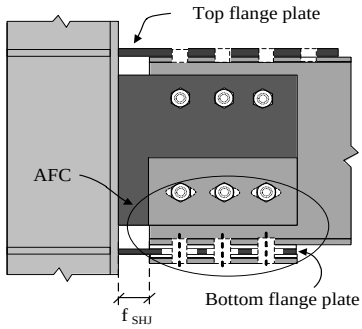

Figure 1: Sliding Hinge Joint layout.

Further developments on the SHJ have since been undertaken. Clifton [1] and MacRae *et al.* [2] investigated the importance of construction tolerance in the vertical offset between the top and bottom flange plates and MacRae *et al.* [2] investigated the effects of aluminium and mild steel shims compared to brass shims tested by Clifton [1]. It was shown that a tolerance of 3 mm was sufficient to limit effects on the joint capacity and mild steel shims performed similarly to brass shims. Mild steel shims have since been used in construction. Khoo *et al.* [3] tested steel shims of different hardness, recommending the use of high hardness abrasion resistant steel shims. The particular steel grade used was Bisplate 400, manufactured by Bisalloy Steel Group Limited, Unanderra, Australia [4] and has a specified hardness of 370-430 HB in the Brinell scale.

[1] *PhD Candidate, Department of Civil and Environmental Engineering, University of Auckland, Auckland*

[2] *Lecturer, Department of Chemical and Materials Engineering, University of Auckland, Auckland*

[3] *Associate Professor, Department of Civil and Environmental Engineering, University of Auckland, Auckland*

[4] *Associate Professor, Department of Civil and Natural Resource Engineering, University of Canterbury, Christchurch*

Further work has confirmed the benefits of high hardness shims [5]. Research is currently underway to implement the AFC in other seismic resistant systems [5, 6], and to develop a self-centering version of the SHJ [7, 8].

It is expected that the SHJ would require limited maintenance following a DLE shaking. This would involve replacing or retightening of the bolts in the AFC, with all other components left in service. The SHJ may then be subject to additional severe earthquake shaking, such as occurred in the 2010 and 2011 Christchurch earthquake sequence. However, prior to this research, there have been no studies on the performance of the bottom and top flange plate components under multiple earthquakes. These components consist of welds and plates which are subject to inelastic demand during joint rotation. In addition, it is also required that the top flange plate does not undergo net elongation during joint rotation in order to function as an effective pin and limit damage in the floor slab.

For the reasons stated above, there is a need to determine whether the flange plate components are likely to be susceptible to low-cycle fatigue fracture in the earthquakes they are expected to experience over their life. This paper presents research undertaken to investigate the resilience of the flange plate components, and in particular, provide answers to the following questions:

1. How do the bottom and top flange plates, and the welds connecting them to the column flange behave under joint inelastic rotation?
2. Are the bottom and top flange plates susceptible to low-cycle fatigue?
3. Is the top flange plate prone to net elongation?
4. Are the current design provisions [1] for the bottom and top flange plates adequate?

2. DESIGN CONSIDERATIONS AND BEHAVIOUR OF THE BOTTOM AND TOP FLANGE PLATES

2.1 Design philosophy

The key flange plate design considerations are the size of the plates, welds, and clearance between the column flange and beam end (f_{SHJ}). The design considerations are briefly presented, with further details found in Clifton [1].

The rotational behaviour of the SHJ under pure positive and negative inelastic rotation (ie. no shear) and AFC sliding is shown in Figure 2, where the bottom and top flange plates are subjected to axial and bending actions. The beam is also subjected to vertical shear demands, which are designed to be resisted by the web plate. Note that the web plate and shear effects are not shown in Figure 2, but are covered in more detail in Section 2.2. The bottom flange plate resists the total sliding shear capacity of the bottom flange bolts, which is calculated as the *number of bolts in the bottom flange plate* × *bolt sliding shear capacity*. The bottom flange plate is sized to suppress: (1) tension yield prior to the full sliding capacity reached, (2) tension fracture while sliding, (3) compression yielding or buckling while sliding and (4) bolt shear fracture. For the first two conditions, the section of the plate adjacent to the reduced cross-sectional area at the bolt holes is critical. Compression buckling of the bottom flange plate must be suppressed for the longest length between the column flange and beam end, which occurs at load reversal from the design positive rotation as shown in Figure 2(a).

The top flange plate anchors the beam to the column and operates as a pin which the column rotates about. The plate is designed to resist the combined sliding shear capacity generated in the bottom web and bottom flange plate AFCs. The plate is sized to suppress net tension yield as well as

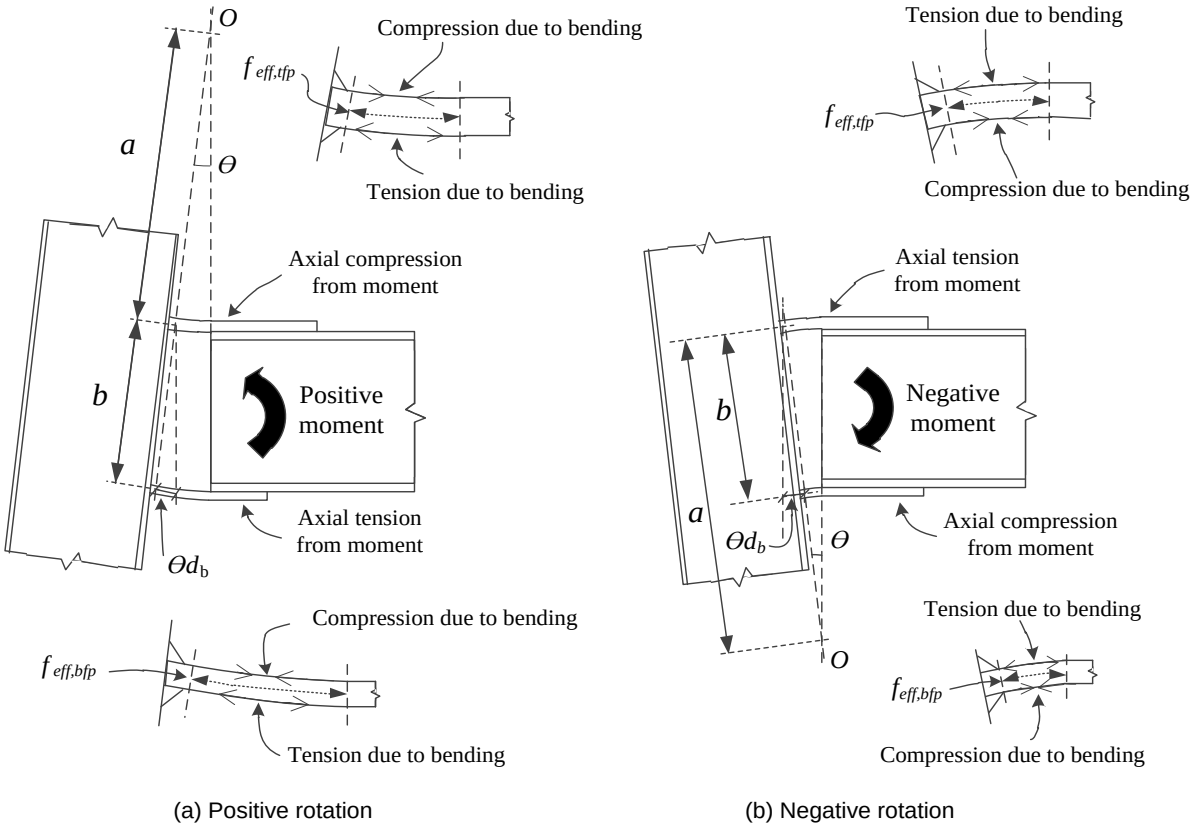

Figure 2: Joint rotation (web plate not shown for clarity).

compression buckling assuming no concrete slab is present. The critical section for local effects is again the reduced cross-sectional area where the top flange plate is bolted to the beam. As such, both bottom and top flange plates away from the bolted region will remain elastic under pure axial loading developed under the design moment capacity.

The flange plates are welded to the column through equal sized fillet welds on both sides of the plates up to a weld length (t_w) of 12 mm. If a t_w greater than 12 mm is required, the design recommendations [9] specify a complete penetration butt weld (herein referred to as a butt weld). The welds are to be Category SP welds in accordance to the provisions of NZS 3404 Steel Structures Standard [10], which specifies welds within the limits of AS/NZS 1554:1 [11]. The welds are subjected to axial loading as well as bending action due to joint rotation.

A critical consideration in the design of the flange plates is the clearance between the column face and the beam end (f_{SHJ}), which is illustrated in Figure 1. In the original development of the SHJ [1], it was found that without sufficient clearance, the bottom flange plate was subject to very high localised curvature when the gap between the column face and the beam flange was at a minimum under negative rotation. This caused significant prying of the bolts due to deformation incompatibility between the sloping face of the column and the horizontal face of the beam, leading to excessive loss of bolt tension and sliding shear capacity. A revised procedure to determine f_{SHJ} was then empirically developed by Clifton [1]. This is presented in Equation 1. It was shown experimentally to ensure the flange plates describe an arc under joint inelastic rotation, allowing the SHJ to develop stable sliding resistance with limited strength degradation. The procedure was then verified through further large-scale testing by Mackinven [12] and Khoo *et al.* [7].

$$f_{SHJ} = t_w + 1.25\theta_d d_b + 2.5t_{bfp} \quad (1)$$

where t_w = weld length;
Θ_d = design rotation;
d_b = beam depth; and
t_{bfp} = thickness of bottom flange plate.

2.2 Demand

The critical components are the welds connecting the plates to the column flange and the plates themselves. As briefly described in Section 2.1, the demands are due to (1) axial and bending actions from joint rotation and (2) vertical shear slip. The welds are required to resist axial and bending loads, which are similar to the welds in beam flanges in traditional welded connections. The flange plates are subjected to longitudinal strain (ε_1) from the axial load due to moment demand and strain due to bending in the weak axis, and shear strain (ε_2) from joint shear slip deformation demands.

The axial load from moment demand results in longitudinal axial strain (ε_a) which cycles in tension and compression, depending on the direction of moment. Under positive (anti-clockwise) rotation, the top flange plate is in compression (negative ε_a), while the bottom flange plate is in tension (positive ε_a). Under negative (clockwise) rotation, the top flange plate is in tension (positive ε_a), and the bottom flange plate is in compression (negative ε_a). The magnitude of ε_a is dependent on the moment demand (M), distance between the flange plates (d), plate cross-sectional area (A) and elastic modulus (E). The ε_a can be calculated with Equation 2, which assumes the axial stress and strain to be uniformly distributed through the cross-sectional area of the flange plates. Based on the design methodology of suppressing axial yielding in the critical section of the plate (ie. reduced cross-sectional area due to bolt holes), the full cross-section of the top flange plate is expected to be under axial yield strain of 0.15% determined for Grade 300 steel to NZS 3404 [10]. The analysis in this paper assumes ε_a = 0.15% in order to a give a conservative estimate of the flange plate cycle lives.

$$\varepsilon_a = \pm\frac{M}{dAE} \quad (2)$$

where ε_a = axial strain;
M = moment demand;
d = beam depth;
A = plate cross-sectional area; and
E = elastic modulus.

The formation of the arc also induces longitudinal strain in the bottom and top flange plates due to bending (ε_b). The level and direction of strain ε_b is dependent on the level and direction of rotation, which from geometrical considerations is taken about a point O, at a distance L from the plate of interest as shown in Figure 2. The position of O changes based on the direction of loading, whereby it is above the joint under positive rotation, and below the joint under negative rotation. The magnitude of length L differs for the bottom and top flange plates. For the bottom flange plate, $L = a + b$ and $L = a - b$ under positive and negative rotations respectively. For the top flange plate, $L = a$ under both positive and negative rotations. The respective lengths are shown in Figure 2. Length L for both bottom and top flange plates are nevertheless dependent on the rotation (Θ) and effective length of curvature (f_{eff}) of the plate of interest, and can be calculated by geometry. Length f_{eff} is the effective length of the plate curving about point O, excluding weld lengths and sliding distance. This length is described in more detail in Section 4.2. The magnitude of bending strain (ε_b) increases the further the fibres are from the neutral axis, making the maximum strain also a function of the plate thickness. This is shown in Equation 3, which calculates the actual length (l) of the extreme fibre under rotation, consisting of the effective clearance (f_{eff}), and the deformation (Δl) calculated in Equations 4 and 5 respectively, The strain demand ε_b is then calculated with Equation 6, based on the ratio between the effective length of curvature and the plate thickness (r) calculated in Equation 7.

The longitudinal strain demand (ε_1) is the combined maximum ε_a and ε_b, and can thus be calculated with Equation 8. The ε_1 distribution over the cross-sectional area of the plates are presented in Figure 3 for both the bottom and top flange plates under positive and negative rotations. Assuming a design rotation of 30 milliradians (mrad), the resulting strain can be related to the ratio $r = f_{eff}/t_p$. This is presented in Figure 4(a), showing the decrease in strain demand as r increases. The ε_1 shown in Figure 5(a) was calculated assuming an ε_a of 0.15%. The design rotation of 30 mrad was determined from the plastic collapse rotation in a beam at 2.5% drift (NZS 1170.5 [13]), with a non-uniformity factor of 1.2. It has been a key value used in connections for seismic resistance in ductile detailing of steel structures for fire and earthquake resistance [9]. This is also consistent with the findings of the SAC Joint Venture [14] which predicted a 95th percentile demand of 3.0% interstorey drift in the critical stories of steel MRFs under a DLE. This was determined through a large number of non-linear time-history analyses on buildings of varying heights. Furthermore, the 30 mrad design rotation would provide a conservative estimate of the SHJ low-cycle fatigue life as the actual joint rotation would be less than 30 mrad under 3.0% drifts.

(a) Bottom flange plate

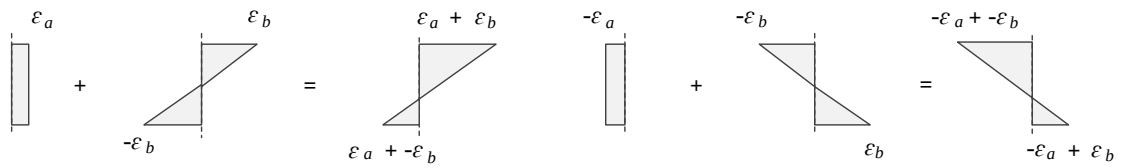

Positive moment Negative moment

(b) Top flange plate

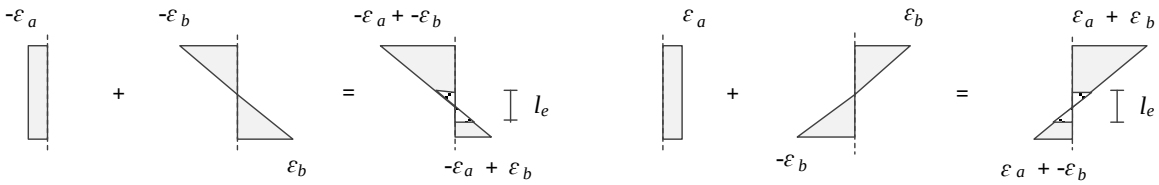

Positive moment Negative moment

Figure 3: ***Longitudinal strain distribution under positive and negative moment for (a) bottom flange plate and (b) top flange plate.***

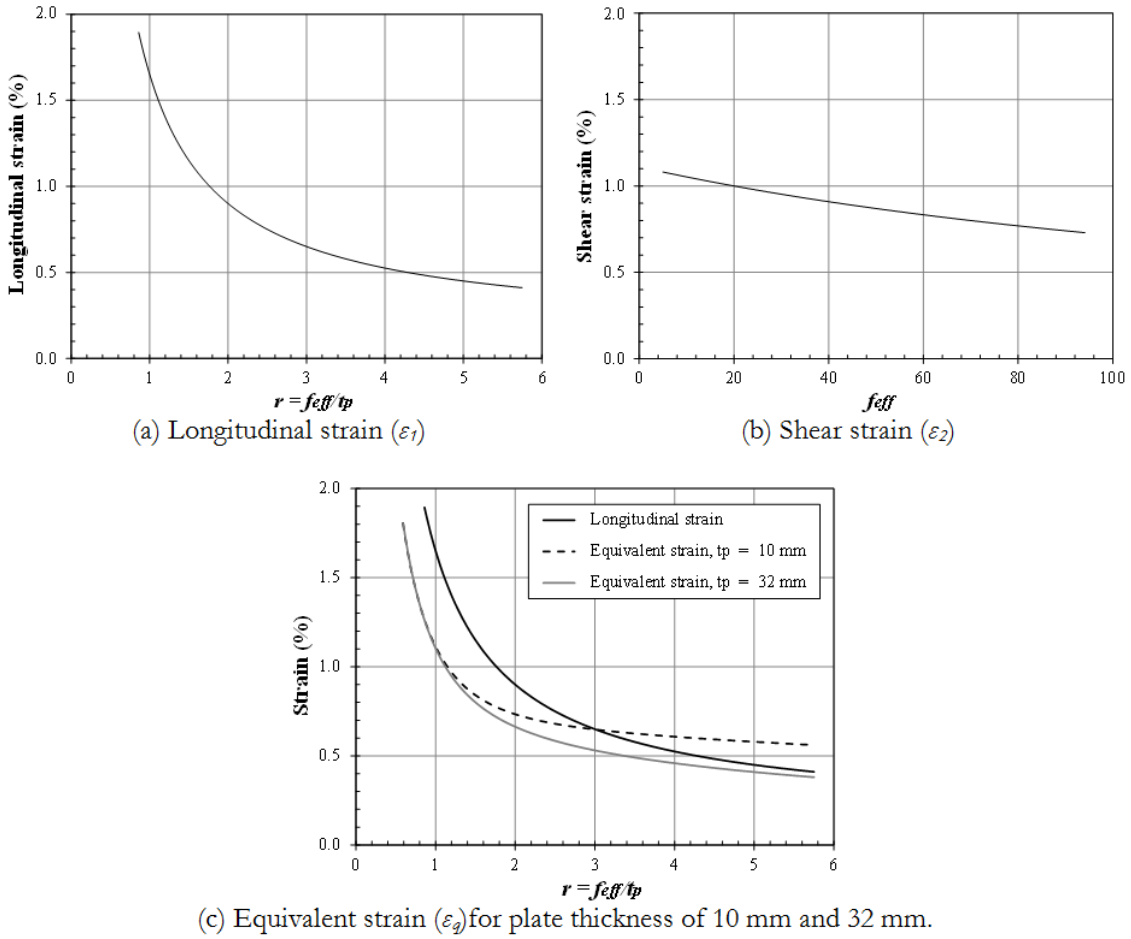

(a) Longitudinal strain (ε_1) (b) Shear strain (ε_2)

(c) Equivalent strain (ε_q)for plate thickness of 10 mm and 32 mm.

Figure 4: ***Strain relationship under 30 mrad design rotation for (a) longitudinal strain and r = f_{eff}/t_p, (b) shear strain and f_{eff} and (c) longitudinal and equivalent strain and r = f_{eff}/t_p.***

$$l = \theta\left(L \pm \frac{t_p}{2}\right) = f_{eff} \pm \Delta l \quad (3)$$

$$\tan\theta \approx \theta = \frac{f_{eff}}{L} \rightarrow f_{eff} = \theta L \quad (4)$$

$$\Delta l = \pm\frac{\theta t_p}{2} \quad (5)$$

$$\varepsilon_b = \pm\frac{\theta}{2r} \quad (6)$$

$$r = \pm\frac{f_{eff}}{t_p} \quad (7)$$

$$\varepsilon_1 = \varepsilon_a + \varepsilon_b \quad (8)$$

where l = actual length of extreme fibres;
Θ = rotational demand;
t_p = plate thickness;
f_{eff} = effective length of curvature;
Δl = plate deformation
r = ratio between effective length and plate thickness ε_b = plate strain due to bending, and
ε_1 = plate longitudinal strain.

The SHJ resists vertical shear through the web plate. The shear deformation (Δ_s) considered is therefore that due to vertical slip of the beam relative to the web plate, which is resisted by the top web bolt group.

The top web bolt group holes are standard 2 mm oversized holes, corresponding to the maximum slip (Δ_m) assuming the bolts were bearing on the opposite end to the direction of slippage at installation. As the beam effectively rotates about the column and web plate, the Δ_s is the relative slip at the beam end, which is less than the slippage at the bolts. The Δ_s is calculated through geometry as a function of the relative distances between the column to the beam edge, and the column to the furthest bolt. The distances are related to f_{eff}, the edge distance between the beam end and bolt (e_{ep}) and the distance between the bolts (S_g) as shown in Equation 9 and illustrated in Figure 5(a). The shear strain (ε_2) is a function of f_{eff} and calculated with Equation 10, and illustrated in Figure 5(b). Note that it is assumed that there are three top web bolts and that a_{ep} = 40 mm and S_g = 70 mm, which is the minimum number of bolts required and the minimum allowable distances in design respectively [1], representing the most conservative case. It should also be noted that the presence of a floor slab is likely to provide additional vertical shear resistance and reduce the likelihood of shear deformation. The analysis was nevertheless conducted for the joint without the slab to determine estimates of likely possible demands.

$$\Delta_s = \frac{\Delta_m}{f_{eff} + a_{ep} + 2S_g} \times f_{eff} \quad (9)$$

$$\varepsilon_2 = \frac{\Delta_s}{f_{eff}} \quad (10)$$

$$\varepsilon_q = \frac{\sqrt{(\varepsilon_1 - \varepsilon_2)^2 + (\varepsilon_2 - \varepsilon_3)^2 + (\varepsilon_3 - \varepsilon_1)^2}}{\sqrt{2}(1+\nu)} \quad (11)$$

where Δ_s = shear deformation in flange plates;
Δ_m = maximum slip between beam and web plate, 2 mm adopted;
a_{ep} = edge distance between beam end and top web bolts, 40 mm adopted;
S_g = distance between top web bolts, 70 mm adopted;
ε_1 = longitudinal strain;
ε_2 = shear strain;
ε_3 = third principal strain (equals zero);
ε_q = equivalent strain;
ν = Poisson's ratio, 0.3 adopted for steel.

The combination of longitudinal (ε_1) and shear strains (ε_2) in the flange plates can be considered through the von Mises equivalent strain (ε_q) shown in Equation 11, which can then be compared to uniaxial test results. The relationship between r and ε_q is shown in Figure 4(c), which also shows the relationship with ε_1. As ε_2 is independent of t_p, the ε_q is calculated for t_p of 10 mm and 32 mm, which represent the lower and upper plate thickness limits expected in standard SHJ construction. As for both ε_1 and ε_2, the ε_q demand decreases with increasing clearance f_{eff}. It can also be seen that the demand decreases with increasing t_p. The ε_1 is critical till approximately r = 3 when t_p = 10 mm, after which the ε_q becomes the critical case.

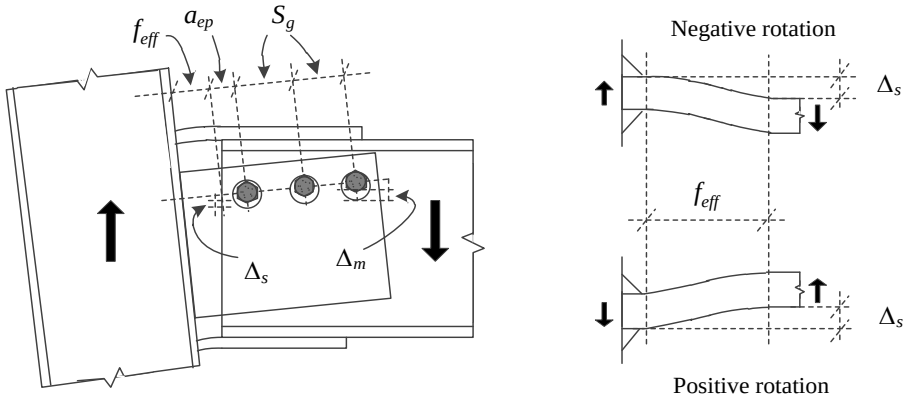

(a) Shear slip under negative rotation (b) Shear deformation

Figure 5: Shear demands (a) slip between beam and web plate under negative rotation and (b) shear deformation in flange plates.

As the joint behaviour is dependent on the two components, namely welds and plates, the weld performance and interaction between the plate and the welds is presented in Section 3, and the performance evaluation of the flange plates is presented in Section 4.

3. WELD BEHAVIOUR

The weld and plate performance was analysed using the results of tests carried out by the Heavy Engineering Research Association (HERA). As part of their seismic research project, HERA carried out a series of small and large scale tests aimed at testing column-beam flange welds in rigid welded connections [15, 16].

The small scale test components comprised a welded T-section (Figure 6), which represented a beam flange welded to a column flange. The objective was to determine whether fracture occurs in the weld or beam flange in welded beam-column connections through testing of T-sections under inelastic cyclic loading. The test rig (Figure 7) was the same rig used by Clifton [1] in his small scale AFC component testing, while a similar configuration was used by Khoo *et al.* [3]. The T-section specimens were installed at the top of the rig shown as *C*, with the actuator applying the load at *B*, rotating the lever arm as it pivots about *A*. The rig simulated the rotation of a beam about the column, loading the specimen dynamically under cyclic tension and compression, with the plate restrained to prevent buckling under compression. Large scale beam-column connection tests were also conducted, simulating connections in exterior moment resisting frames [15]. The large scale tests were undertaken at quasi-static rates of loading.

In both small and large scale tests, the fillet and butt welds were subjected to bending in addition to axial load, in a similar way to the flange plates in the SHJ. They were, however, not subjected to shear strain. The plates were made of Grade 300 mild steel, and can therefore be directly related to the top and bottom flange plates in the SHJ. The test programme included testing double sided fillet welds and butt welds of different filler materials (355 MPa, 400 MPa and 470 MPa yield strengths). This was done to vary the ratio of the weld metal strength to the parent metal strength (which was mild steel for all tests). The level of weld defects were measured and shown to be within the limits of AS/NZS 1554:1 [11] for Category SP welds. The specimens were tested to failure, which imposed plate strains of up to seven times their yield strain. It was found that when the weld material nominal tensile strength (f_{uw}) exceeded the parent material nominal tensile strength (f_{up}), failure occurred in the plates near the welds for both double sided fillet and butt welds in welded T-sections, showing the adequacy of this provision in forcing failure of the specimen to occur in the plates under inelastic cyclic loading. As the plate and weld conditions in these tests are the same as those in the flange plates of the SHJ and the requirements of $f_{uw} > f_{up}$ applies, it is concluded that the flange plate welds are capable of resisting seismic load and forcing inelastic deformation/failure to occur in the flange plates critical location (ie. near the welds) under multiple cycles of loading, making the flange plates the critical components in this system.

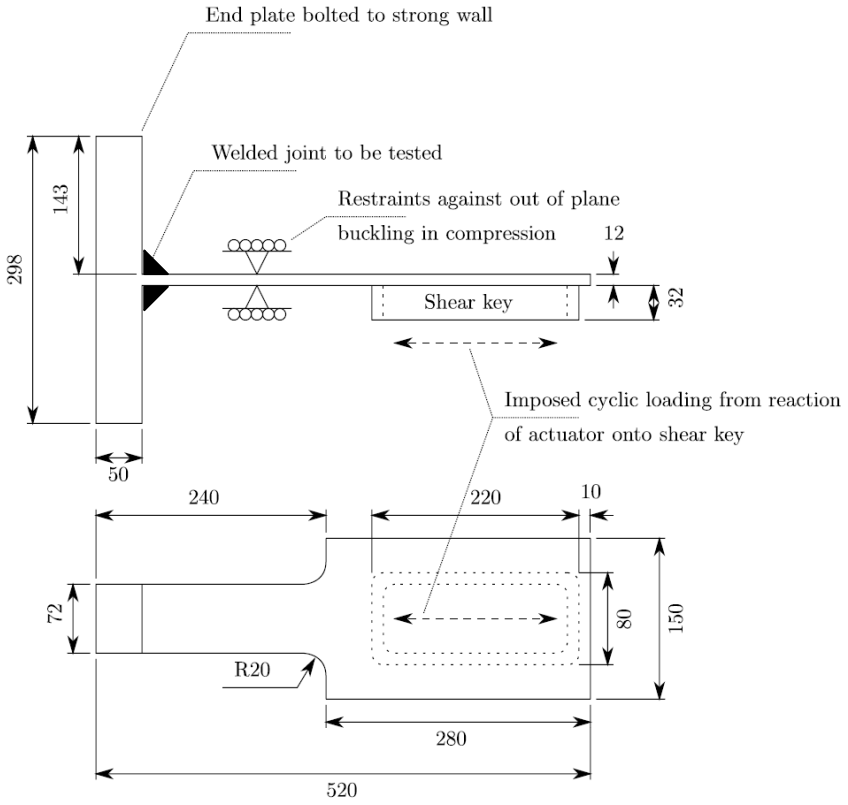

Figure 6: HERA small scale test specimens [17].

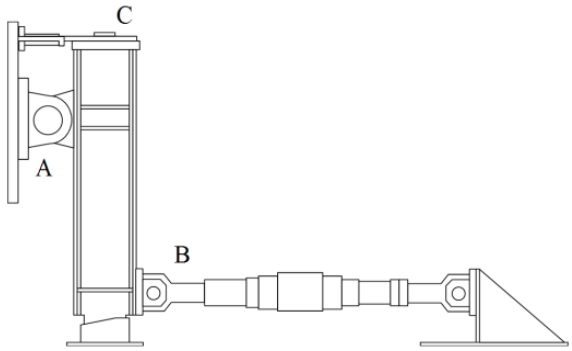

Figure 7: Small scale test rig [3].

4. FLANGE PLATES

4.1 Damage model

The damage model chosen to estimate the number of cycles required to generate low-cycle fatigue failure in the flange plates is based on the well-known Coffin-Manson relationship. This relationship was published by Manson [18] and Coffin [19] showing a linear relationship between plastic strain (Δe_p) and the number of cycles to fracture (N_f) of metallic material subjected to cycle stress in the log-log scale, and has been applied for seismic conditions (eg. [20]). The relationship is presented as:

$$\Delta e_p = n N_f^{\,c} \tag{12}$$

Seal *et al*. [17] applied the Coffin-Manson relationship to the results of six HERA small scale tests undertaken at two different strain conditions [16] with good agreement. In each of the six tests, failure occurred in the plates near the welds, which in this context are assumed to be in the SHJ flange plates. The parameters from that study were n = 0.23 and c = 0.5759, which were provided by Seal [17] through personal communication. However, rather than axial strain (e_{axial}), the model used diametric strain (e_{dia}), which is approximately half the axial strain (ie. $e_{axial} \approx 2e_{dia}$).

The modified Coffin-Manson relationship is shown in Equation 13, which is rearranged to Equation 14 and the results from its application are presented in Figure 8(a), showing the relationship between N_f and e_{axial}. This is used to predict N_f of the top and bottom flange plates by using either the longitudinal (ε_1) or equivalent strain (ε_q) to take the multiaxial strains into account, whichever is the critical case. As the strain demand is related to $r = f_{eff}/t_p$ as shown previously in Figure 4, this can be extended to Figure 8(b) which shows the relationship between N_f and the ratio $r = f_{eff}/t_p$ for t_p = 10 and 32 mm, assuming the joint is loaded to constant cycles to the 30 mrad design rotation. That range of plate thicknesses covers those used in practice. With an r = 1, the joint is expected to fail at approximately N_f = 323 cycles, which is well beyond the expected demand on an MRF connection even in multiple major earthquakes.

It was shown through time-history analyses that steel MRFs on average may be subjected to an equivalent of 22 damaging cycles of drifts between 0.5% to 3.0% under a DLE [14]. The current design recommendations are investigated in Section 4.2.

$$\frac{e_{axial}}{2} = 0.23 N_f^{\,-0.5759} \tag{13}$$

$$N_f = \left(2.174 e_{axial}\right)^{-1.7364} \tag{14}$$

where e_{axial} = axial strain;
N_f = number of cycles to failure.

It should be noted that the parameters in the Coffin-Manson equation may not be fully representative of the actual flange plates in the SHJ, as they were only based on six tests at two different strain conditions as mentioned above. In addition, the Coffin-Manson relationship assumes cyclic demand at constant strains, unlike the variable strain amplitude which occurs in an actual earthquake. It was nevertheless shown in the HERA tests [15] that the accumulation of damage is independent of loading history. Furthermore, Seal *et al*. [17], using toughness as a damage parameter to predict failure in beam flanges subject to inelastic demand under seismic loading, tested steel samples cut from the flanges of 310 UC 158 sections under variable strain amplitudes. The specimens were tested to groups of 10 cycles to approximately 2.5%, 3 cycles to 5% and 1 cycle to 10% axial strain, which were arranged in all six possible orders. It was found that there were no significant differences in damage accumulation between different orders, although there was a slight trend showing lower damage when the regimes started with the largest strain of 10%. This represents possible effects that may be generated

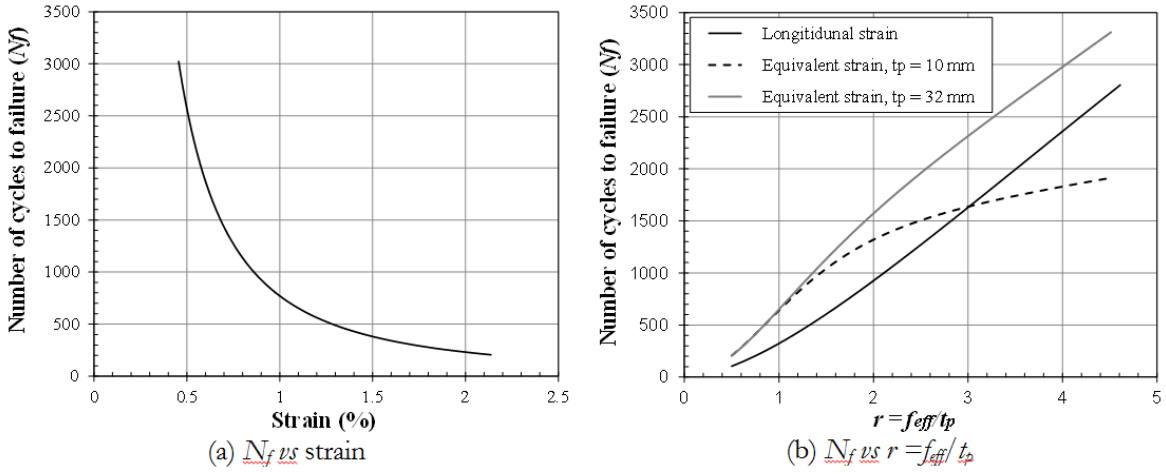

Figure 8: Relationship between number of cycles to failure N_f and (a) strain, and (b) $r = f_{eff}/t_p$ for longitudinal strain and equivalent strain where t_p = 10 and 32 mm.

from near fault effects, and is beneficial in practice given it is the most severe form of earthquake demand. Its application in the flange plates of the SHJ may however be limited given geometric differences in the test specimens. Given these limitations and uncertainties, the numbers calculated by the model described above give indicative limits for low cycle fatigue failure of the flange plates.

4.2 Comparison with design provisions

4.2.1 *Bottom flange plate*

There are two cases for the bottom flange plate, which is the joint under positive and negative moments. Under positive moment, the effective length $f_{eff,bfp}$ is at its maximum as the column rotates away from the beam. This increases the distance L from the point O, which results in a lower level of plate curvature. Under negative moment, $f_{eff,bfp}$ is at its minimum, and therefore L is also at its minimum. The negative moment produces a higher level of curvature compared to positive moment, making it the critical case. The critical length $f_{eff,bfp}$ at this point is then the clearance f_{SHJ} less the weld length (t_w) and sliding distance, and is calculated with Equation 15. Note that the additional distance of flange plate thickness which increases the lever arm above the beam depth (d_b) is considered negligible and not included in the equation. Equation 15 can be combined with Equations 1 and 7, giving an expression of the minimum r ratio (r_{bfp}) shown in Equation 16. This shows that the r_{bfp} for the bottom flange plate would always be above 2.5, and increase as the beam depth increases. With assumed conservative sizes of a 360 UB beam and t_{bfp} = 20 mm, the minimum r_{bfp} is 2.635. The longitudinal strain ε_1 is critical and is expected to fail at N_f = 1,368 cycles to 30 mrad. It should be noted that in reality, the maximum rotation of 30 mrad would only occur once or at most twice under a severe ground shaking. However, this approach was taken to give the most critical case.

$$f_{eff,bfp} = f_{SHJ} - t_w - \theta d_b \tag{15}$$

$$r_{bfp} = \frac{\left(t_w + 1.25\theta d_b + 2.5t_{bfp}\right) - t_w - \theta d_b}{t_{bfp}} \qquad r_{bfp} \geq \frac{0.25\theta d_b}{t_{bfp}} + 2.5 \tag{16}$$

4.2.2 *Top flange plate*

The effective length ($f_{eff,top}$) of the top flange plate is the same under both positive and negative rotations. As sliding does not occur, it is the clearance less the weld length and is calculated with Equation 17. Combining this with Equations 1 and 7 as for the bottom flange plate, this gives an expression of r shown in Equation 18. This gives r_{tfp} as a function of the thickness of the bottom flange plate (t_{bfp}), which is sized independently from the top flange plate.

In order to simplify the analysis, it was assumed that the top flange plate thickness is double that of the bottom flange plate, giving $t_{tfp} = 2t_{bfp}$. In practice, this would not be the case as the top flange plate is sized to the combined sliding shear capacities of both bottom web and bottom flange AFCs as described in Section 2.1, which would be less than double the bottom flange AFC (which provides the joint primary resistance). However, the assumption is conservative in terms of the fatigue life predicted. This simplifies Equation 18 to Equation 19. As for the bottom flange plate, the minimum r_{tfp} is calculated to be 1.672, assuming conservative estimates of a 360 UB beam, and t_{tfp} = 32 mm. The longitudinal strain ε_1 is critical, and equates to a predicted N_f = 712 cycles to a rotation of 30 mrad before failure occurs, making the top flange plate the critical component of the two flange plates.

$$f_{eff,tfp} = f_{SHJ} - t_w \tag{17}$$

$$r_{bfp} = \frac{\left(t_w + 1.25\theta d_b + 2.5t_{bfp}\right) - t_w}{t_{tfp}} \qquad r_{bfp} = \frac{1.25\theta d_b + 2.5t_{bfp}}{t_{tfp}} \tag{18}$$

$$r_{tfp} \geq \frac{1.25\theta d_b}{t_{tfp}} + 1.25 \tag{19}$$

As described in Section 4.1, the values calculated are only indicative due to the uncertainty over the current available damage model. This is nevertheless mitigated by the conservative approach in calculating strain demand, and the calculated numbers of cycles to failure, which is much larger than would be experienced by a structure in service. Applying a factor of safety of 5, which is a conservative value for fatigue determination (Clause 10.1.6 in NZS 3404), this gives a design fatigue life of 142 cycles to 30 mrad of rotation. This is approximately 6.5 times that expected in a DLE, assuming a demand of 22 cycles to 30 mrad rotation, which is itself conservative. While the state of knowledge is not sufficient to predict a seismic endurance limit with confidence, it is sufficient, with suitably conservative assumptions on the number and magnitude of loading cycles as has been made, to be confident that well designed and detailed flange plates will not fail under low cycle fatigue. The design provisions for the flange plates are therefore adequate, and changes are not required.

5. TOP FLANGE PLATE ELONGATION

The other potential issue requiring review is the possibility of the top flange plate undergoing net elongation. It was found from previous large scale tests of subassemblies both with and without slabs [1, 7], that there was no measureable or visible elongation in the top flange plates. This is due to the behaviour under both positive and negative rotations and the resulting longitudinal strain distribution and neutral axis position. The longitudinal strain distribution is shown in Figure 3. As described in Section 2.2, under positive rotation, axial compression is generated due to the SHJ moment demand, while plate bending due to joint rotation causes a compressive strain at the top extreme fibre and a tension strain at the bottom. This shifts the neutral axis downwards away from the centre, and leaves a portion of the plate elastic, shown as l_e. Under negative rotation, the actions are the opposite, with the SHJ moment demand causing a net axial tension, and the plate bending causing a tension at the top extreme fibre and compression at the bottom. This also shifts the neutral axis downwards as is the case shown in Figure 9. This behaviour is ideal as the neutral axis and resulting l_e remains at the same location under both positive and negative rotations, leaving a core area elastic and preventing net elongation in the plate. The length l_e and the percentage of elastic area over the thickness of the plate (P_{el}) are derived below in Equations 20 and 21. In order to achieve a P_{el} > 10%, which is the minimum considered necessary to prevent elongation, the ratio of $r = f_{eff,tfp}/t_{tfp} > 1$ is required. This assumes that if 10% of the core remains elastic, there would be no net elongation. In practice, $r = f_{eff,tfp}/t_{tfp} > 1.25$ will occur in design of the SHJ, and therefore no further design requirements are required to prevent top flange plate elongation.

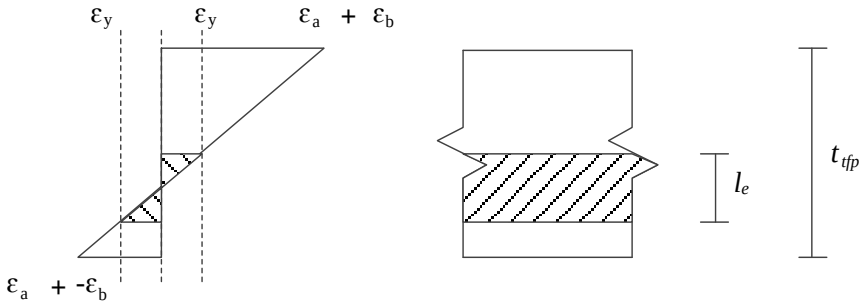

Figure 9: Top flange plate core elastic area under negative rotation.

$$l_e = 2\varepsilon_y \times \frac{t_{tfp}}{2\varepsilon_{b,tfp}} = 2\varepsilon_y \times \frac{t_{tfp}}{2(\theta/2r)} = \frac{2\varepsilon_y f_{eff,tfp}}{\theta} \quad (20)$$

$$P_{el} = \frac{l_e}{t_{tfp}} \times 100 = \frac{200\varepsilon_y r}{\theta} \quad (21)$$

6. CONCLUSIONS

Analysis of the bottom and top flange plate behaviour in the SHJ under inelastic rotation was conducted using previous experimental studies. It was found that:

1. Previous testing by HERA has shown that welds designed to NZS 3404 seismic design provisions do not become inelastic, making the plates the critical component for low cycle fatigue checks. The basic flange plate deformation as the beam end rotated was approximated by an arc. The effects of shear slip on this were considered in order to obtain estimates of the likely possible demands in the critical location near the weld.
2. Under the minimum f_{SHJ} based on the current design recommendations, the SHJ can undergo at least 6 design level earthquake events, each with 22 cycles to an inelastic sliding rotation of 30 mrad (with a safety factor of 5), before the top flange plate is predicted to fail in low-cycle fatigue.
3. The rotational behaviour of the top flange plate and resulting strain distribution ensures a core area remains elastic under joint inelastic rotation if there is no shear deformation. The current design procedure requires the core area to be at least 10%, and therefore the top flange plate is not expected to undergo net elongation.
4. Design procedures specified by Clifton [1] for the bottom and top flange plate requiring a minimum clearance f_{eff} are adequate and do not require any changes to account for low-cycle fatigue issues presented in this paper.

REFERENCES

1 Clifton, G.C. (2005). "Semi-rigid joints for moment-resisting steel framed seismic-resisting systems." Department of Civil and Environmental Engineering, University of Auckland, Auckland.

2 MacRae, G.A., Clifton, C., MacKinven, H., Mago, N., Butterworth, J. and Pampanin, S. (2010)."The Sliding Hinge Joint moment connection". *Bulletin of the New Zealand Society for Earthquake Engineering* **43** (3): 202-212.

3 Khoo, H.H., Clifton, C., Butterworth, J.W., MacRae, G.A. and Ferguson, G. (2012). "Influence of steel shim hardness on the Sliding Hinge Joint performance". *Journal of Constructional Steel Research* **72** (0): 119-129.

4 Bisalloy Steels (2008). Bisplate Technical Guide. Unanderra, Australia.

5 Chanchi-Golondrino, J., MacRae, G.A., Chase, J.G., Rodgers, G.W., Mora-Munoz, A. and Clifton, C. (2012). "Design considerations for braced frames with asymmetrical friction connections – AFC". *7th STESSA Conference on the Behaviour of Steel Structures in Seismic Areas*. Santiago, Chile.

6 Khan, M.J. and Clifton, C. (2011). "Proposed development of a damage resisting eccentrically braced frame with rotational active links". *Bulletin of the New Zealand Society for Earthquake Engineering* **44** (2): 99-107.

7 Khoo, H.H., Clifton, C., Butterworth, J.W. and MacRae, G.A. (2012). "Experimental studies of the self-centering Sliding Hinge Joint". *2012 NZSEE Conference*. Christchurch, New Zealand.

8 Khoo, H.H., Clifton, C., Butterworth, J.W., MacRae, G.A., Gledhill, S. and Sidwell, G. (2012). "Development of the self-centering Sliding Hinge Joint with friction ring springs". *Journal of Constructional Steel Research* **78** (2012): 201-211.

9 Steel Construction New Zealand (2007). Steel Connect SCNZ: Parts 1 and 2. Auckland, New Zealand.

10 Standards New Zealand (2009). NZS 3404 - Steel Structures Standard. Wellington, New Zealand.

11 Standards New Zealand (2011). AS/NZS 1554.1 – Structural Steel Welding Part 1: Welding of steel structures. Wellington, New Zealand.

12 MacKinven, H. (2006). "Sliding Hinge Joint for steel moment frames experimental testing". ENCI 493 Project Report. Department of Civil Engineering, University of Canterbury, Christchurch.

13 Standards New Zealand (2004). NZS 1170.5 – Structural Design Actions. Earthquake Actions. Wellington, New Zealand.

14 SAC Joint Venture (2000). "Loading histories for seismic performance testing of SMRF Components and Assemblies". Rep. No. SAC/BD-00/10. Stanford University, California.

15 Eisenbeis, M., Scholz, W., Clifton, C. and Bayley, C. (2000). “Development of small scale test rig to trial the performance of welded beam to column connections under seismic loading”. R8-18. Heavy Engineering Research Association. Auckland.

16 Mago, N., Seal, C.K., Scholz, W., Clifton, C. and Bauer, S. (2001). “Cyclic performance of welded T joints”. Heavy Engineering Research Association. Auckland, New Zealand.

17 Seal, C.K., Hodgson, M.A., Clifton G.C. and Ferguson W.G. (2009). "A novel method for predicting damage accumulation in seismically deformed steel". *Journal of Constructional Steel Research* **65** (12): 2157-2166.

18 Manson, S.S. (1953). “Behaviour of materials under conditions of thermal stress”. *Heat Transfer Symposium*, University of Michigan Engineering Research Institute, Ann Arbor, Michigan.

19 Coffin, L.F.J. (1954). "A study of the effects of cyclic thermal stresses on a ductile metal". *Trans. ASME* **76**: 931-950.

20 Kasai, K. and Xu, Y. (2003). "Cyclic behaviour and low-cycle fatigue of semi-rigid connections". *5th STESSA Conference on the Behaviour of Steel Structures in Seismic Areas*. Naples, Italy.